



## Design, Numerical Simulation and Experimental Investigation of Radial Inflow Micro Gas Turbine

S. P. Shah<sup>1†</sup>, S. A. Channiwala<sup>2</sup>, D. B. Kulshreshtha<sup>1</sup> and G. C. Chaudhari<sup>1</sup>

<sup>1</sup> Mechanical Engineering Department, C. K. Pithawalla College of Engineering and Technology, Surat – 395007, India

<sup>2</sup> Mechanical Engineering Department, S V National Institute of Technology, Surat – 395007 India

†Corresponding Author Email: [samip\\_mech@yahoo.com](mailto:samip_mech@yahoo.com)

(Received October 23, 2018; accepted January 28, 2019)

### ABSTRACT

The work arose initially from an interest in design of radial turbine for small scale gas turbine applications typically suitable for distributed power generation system which demands compact installations. The paper describes an investigation in to the design and performance of radial inflow turbines having a capacity of 25kW at 1,50,000 rpm. First a non-dimensional design philosophy is deduced to design a turbine rotor. The design approach is largely one dimensional along with empirical correlations for estimating losses used to obtain the main geometric parameters of turbine. From the proposed design approach, turbine total-to-static efficiency is calculated as 84.91% which is reasonably good. After that a modified vortex design procedure is developed to derive the non-dimensional volute geometry as a function of azimuth angle for actual flow condition. Once a specific turbine is designed, the flow is analyzed in detail using a three-dimensional Computational Fluid Dynamics (CFD) code in order to assess how accurately the performance is predicted by simple meanline analysis. Finally, a fully instrumented experimental setup is developed. The experimental investigations have been carried out to study the temperature and pressure distribution across turbine and total-to-static efficiency is calculated. The limitations of surging and choking in compressor as well as in the bearings to take up load at such high speed has allowed the tests to be conducted upto 70000 rpm only, with turbine inlet temperatures ranging from 900 K to 1000 K and a pressure ratio upto 1.79, which developed power in the range of 1.69 kW to 10.22 kW. The uncertainty bands are in order of  $\pm 13.76\%$  to  $\pm 3.12\%$ . It is observed that the CFD results are in good agreement with test results at off design condition. CFD models over predicted total to static efficiency by order of 7-8% at lower speed. These deviations are reduced as turbine runs close to design point.

**Keywords:** Turbine design; Volute design; Small gas turbine; Radial turbine; Alternate design.

### NOMENCLATURE

$b$	blade width	$m_R / m (X)$	recirculating mass
$C$	absolute velocity	$N$	speed of rotation
$C_\theta$	whirl velocity	$N_S$	specific speed
$C_s$	isentropic velocity	$P$	pressure, bar
$C_m$	mean velocity	$p$	constant
$C_v$	specific heat at constant volume	$r$	radius
$C_w$	relative velocity	$r_{3s}/r_2$	radius ratio
$C_f$	friction coefficient	$S_w$	non dimensional power ratio
$d$	diameter	$S$	swirl co efficient
$D_s$	specific diameter	$T$	temperature
$h$	enthalpy	$U$	blade speed
$k$	constant	$W_R$	relative velocity ratio
$L$	passage length	$Z_B$	Number of blades
$L_h$	hydraulic length	$\alpha$	absolute flow angle.
$D_h$	hydraulic diameter	$\beta$	relative flow angle.
$M$	Mach Number	$n$	Specific heat ratio
$m$	mass flow rate, exponent	$\eta$	Efficiency

$\rho$	density	$\Delta\phi$	angular change
$\delta$	trapezium wall angle		
$\phi$	flow coefficient, azimuth angle	<b>Subscripts</b>	
$\psi$	blade loading coefficient	0	stagnation, Stator inlet
$\theta$	dimensionless mass flow rate	1	turbine inlet
$\Delta q_f$	passage loss	2	rotor inlet
$\Delta q_{CL}$	tip clearance losses	3	rotor exit
$\Delta q_{bl}$	blade loading loss	h	hub
$\Delta q_k$	passage curvature loss	n	nozzle
$\Delta q_{ex}$	discharge Kinetic energy loss	s	shroud
$\Delta q$	total loss	ts	total to static
		tt	total to total
		v	volute

## 1. INTRODUCTION

By the end of the 1950s the usefulness of the 1-D approach had been reasonably well documented and discussed for design of radial turbine. A review of design considerations included loss predictions, method of finding the optimum number of rotor blades, optimum blade spacing and the role of cross-passage pressure gradients in blade loading loss. An important contribution to practical design methods came from Balje (1962), Rodgers (1987a) and Chen and Baines (1994). Balje's study was focused on similarity relations and produce performance charts for range of turbine types in which geometry was defined as function of specific (Ns) and specific diameter (Ds). With a strong practical content, Rodgers (1987a) provided a useful reference in his review of radial and mixed flow turbine design option. He correlates turbine efficiency with isentropic velocity ratio and flow coefficient. Later, Chen and Baines (1994) developed the design in lieu to Whitfield (1989) to produce a method for optimizing radial and mixed flow turbine designs. They introduced loading coefficient as a key design parameter and produced a chart to correlate it with flow coefficient. The experimental publications in 1960s to 1970s to evaluate optimum rotor dimensions concluded that a value of about 0.1 was optimum for the ratio of rotor inlet width to inlet diameter whereas; Watanabe *et al.* (1971) suggested 0.07 to 0.088. They also studied the effect of ratio of rotor inlet diameter to average exit diameter, whose value ranged from 1.6 to 2.2 for obtaining the best performance point, which agrees well with the optimum range reported by Rodgers (1987b). The radial turbine rotor design procedure developed by Balje (1962), Rodgers (1987a) and Baines and Chen (1994), however, is restricted by the application of charts they developed. To overcome this problem, in this paper the alternate design methodology is suggested in which the rotor dimensions is non-dimensionalized by the rotor inlet radius, and the fluid and rotor inlet and outlet velocities by the inlet stagnation speed of sound. For given mass flow rate and the inlet stagnation temperature and

pressure, it will then be possible to convert these to the actual dimensions and velocities.

The number of publications relating to volute design appears to have risen significantly from the 1980s. A simple but common approach relied on the assumption of free vortex flow and uniform reduction of mass flow around the volute. Whitfield *et al.* (1991, 1994) introduced a 1-D volute design procedure, in which flow deviates from true free vortex and accounts for the dissipation of angular momentum and energy. To support this, MacGregor *et al.* (1994) reported comprehensive measurements from turbocharger volute. The main findings were that the assumption of free vortex was only felt to be valid over the first 180° while, on the later part of volute flow free vortex flow must be modified to achieve a fair correlation with experiments. F. Gu *et al.* (2001) proved theoretically that the incompressible approach fails to provide a free vortex and uniform flow for the wheel in compressible flow regimes and observed that A/r ratio predicted by incompressible approach is larger than the compressible approach. An extensive performance investigation has been conducted on a radial turbine with three vaneless volutes and three corresponding vaned stators by Spence *et al.* (2007) and found under all operating conditions, vaneless volutes delivered a higher efficiency over the vaned stators. Later, researchers also proved that the incompressible approach fails to provide a free vortex and uniform flow for the wheel in compressible flow regimes. As the flow at inlet section to turbine rotor is compressible, the free vortex assumptions cannot be applicable. Accordingly, a design procedure has been developed to derive the non-dimensional volute geometry in terms of flow area and radius ratio as a function of azimuth angle for actual flow conditions.

## 2. ALTERNATE DESIGN METHODOLOGY

### 2.1 Rotor Design

As mentioned previously, the inlet velocities are

non-dimensionalized by the inlet stagnation speed of sound and the exit velocities by the exit speed of sound. Since the corresponding temperature ratios are available, the exit velocities can be modified to non-dimensionalized them with the inlet stagnation speed of sound, thereby bringing all the velocities to a common base. Table 1 summarized derived major equations to convert velocity triangles and other parameters in nondimensional forms. Initially efficiencies are assumed but later modified through the specification of empirical losses as, along with the flow passes through turbine stage, entropy generation occurs due to different losses in blade passage. In order to incorporate entropy generation in alternate design methodology the different loss models available in literatures (Spence (2007), Baines (1996), Glassman (1976), Rohlik (1975), Atkinson (1998), Wei (2014), Rogers (1987b), Hiatt (1963)) are studied in depth. Finally, selected loss models are converted in non-dimensional form and produced in Table 1.

**Table 1 Rotor inlet and outlet non-dimensional equations and loss models**

Rotor Inlet	Rotor Outlet
$M_2^2 = \frac{M_{02}^2}{1 - \left(\frac{\gamma-1}{2}\right) * M_{02}^2}$	$\frac{C_3}{a_{03}} = \left(\frac{C_{W3}}{a_{03}}\right) * \cos \beta_3$
$\frac{C_{\theta 2}}{a_{01}} = \left(\frac{C_2}{a_{01}}\right) * \sin \alpha_2$	$M_3 = \left(\frac{C_3}{a_{03}}\right) * \sqrt{\frac{T_{03}}{T_3}}$
$\frac{C_{m2}}{a_{01}} = \left(\frac{C_2}{a_{01}}\right) * \cos \beta_2$	$\frac{C_3}{a_{01}} = \left(\frac{C_3}{a_{03}}\right) * \sqrt{\frac{T_{03}}{T_{01}}}$
$\frac{C_{W2}}{a_{01}} = \left(\frac{C_{m2}}{a_{01}}\right) / \cos \beta_2$	$\frac{C_{W3}}{a_{01}} = \left(\frac{C_{W3}}{a_{03}}\right) * \sqrt{\frac{T_{03}}{T_{01}}}$
$\frac{U_2}{C_{\theta 2}} = \frac{U_2}{a_{01}} / \frac{C_{\theta 2}}{a_{01}}$	$\frac{U_3}{a_{01}} = \left(\frac{U_3}{a_{03}}\right) * \sqrt{\frac{T_{03}}{T_{01}}}$
<b>Loss Models</b>	
$\Delta q_f = 0.03 \left[ \left(\frac{C_{W2}}{a_{01}}\right)^2 + \left(\frac{C_{W3}}{a_{01}}\right)^2 \right] / 4 \left(\frac{D_h}{L_h}\right) * \left(\frac{U_2}{a_{01}}\right)^2$	
$\Delta q_{CL} = 0.4 \left(\frac{\varepsilon}{b_2}\right) * \left(\frac{C_{\theta 2}}{U_2}\right)^2$	
$\Delta q_{bl} = \left( 2 \left(\frac{C_{\theta 2}}{U_2}\right)^2 / Z_b * \frac{Z}{r_2} \right)$	
$\Delta q_k = \left[ \left(\frac{b_2}{r_2} + \frac{b_3}{r_2}\right) / \left(1 - \frac{r_3}{r_2}\right) \right] * \left(\frac{C_{W2}^2 + C_{W3}^2}{2a_{01}^2}\right) * \left(\frac{a_{01}}{U_2}\right)^2$	
$\Delta q_{ex} = 0.5(C_3/a_{01})^2$	

The flow diagram of complete alternate design procedure is illustrated in Fig. 1. Based on literatures mentioned above and actual cycle analysis design conditions are selected and listed in Table 2. The principal dimensional ratios of the rotor are found by iterating suggested non dimensional equations. The principal dimensional ratios are then transformed to absolute

dimensions through the specification of the inlet stagnation conditions and the mass flow rate of the working fluid (i.e. Designed Condition) and are presented in Table 3. Figure 2 shows the dimensions of turbine in meridional plane. The turbine total to static efficiency by alternate methodology is 84.91% which is reasonably good.

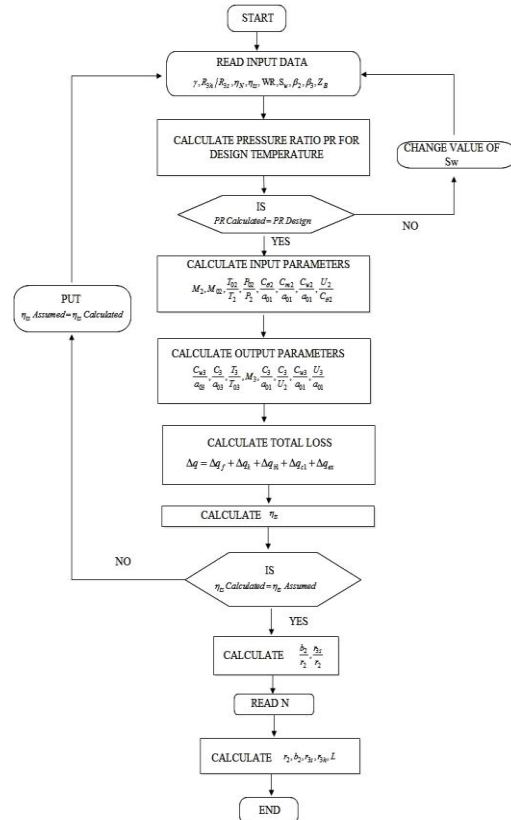


**Fig. 1. Flow diagram of rotor design.**

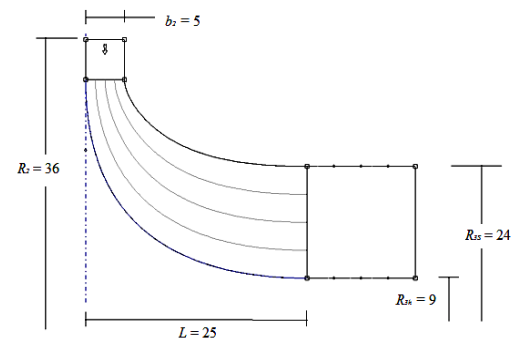


**Fig. 2. Dimensions of radial turbine in Meridional plane (mm).**

After finalizing the turbine rotor dimension, the requirement is to design a volute which gives a desired inlet condition to rotor. The volute of turbine should collect the working fluid, deliver it to turbine rotor as efficiently as possible and provide desired rotor inlet condition. Accordingly, the aerodynamic design of volute follows in next section.

**Table 2 Input parameters and non-dimensional output parameters**

Input Parameters			
$\gamma$	1.302	$S_w$	0.1468
$r_{3h}/r_{3s}$	0.3	$\beta_2$	-38
$\eta_n$	0.9	$\beta_3$	-55
$\eta_{ts}$	0.8491	$Z_B$	12
WR	2		

Output Parameters	
$T_{03}/T_{01}$	0.8531
PR	2.56
$M_2$	0.677
$\alpha_2$	71
$M_3$	0.333
$r_{3s}/r_2$	0.5641
$b_2/r_2$	0.1246
$D_h/L_n$	0.2396
$\Delta q_f$	0.0185
$\Delta q_k$	0
$\Delta q_{bl}$	0.1478
$\Delta q_{cl}$	0.0159
$\Delta q_{ex}$	0.0481
$\Delta q$	0.2304
$\eta_{ts}$	0.8491

**Table 3 Turbine rotor dimensions (Design Conditions: P=25kW,  $\dot{m}=0.1028\text{kg/s}$ ,**

$T_{01}=1200\text{K}$ ,  $P_{01}=2.82\text{bar}$ ,  $N=150,000\text{rpm}$

	Dimension Obtained (mm)	Round off (mm)
$d_2$	71.29	72
$r_2$	35.64	36
$r_{3s}$	23.11	24
$r_{3h}$	8.13	9
$b_2$	4.445	5
L	25	25

## 2.2 Volute Design

Vaneless volute casings are commonly adopted for small and medium size radial inflow turbines. A theoretical investigation based on a one-dimensional compressible flow procedure for a radial inflow turbine volute is used for design. A design procedure has been developed to derive the non-dimensional volute geometry in terms of flow area and radius ratio as a function of azimuth angle.

A uniform acceleration of Mach number with azimuth angle is then assumed in order to develop the non-dimensional design of the volute. The non-dimensional procedure assumes a one-dimensional compressible flow and as such relies on the empirical specification of the dissipation of angular momentum, the dissipation of energy and the deviation of the swirling flow from that of a free vortex. The overall design is then developed to provide the variation of the volute centroid radius and area ratio with azimuth angle.

A circular cross-sectional shape is then used to establish the outer dimensions of the volute. The developed non dimensional equations are solved using a Visual Basic Code for each degree of azimuth angle. The flow diagram for Basic code is shown in Fig. 3.

The derivation of cross-sectional area of volute at volute centre has been derived first through the free vortex assumption using data shown in Table 4 to check the effect of assumed momentum dissipation and % mass flow recirculation near tongue region. The derived radius ratio, area ratio and centroid flow angle are shown as a function of azimuth angle in Figs. 4, 5 and 6, respectively.

**Table 4 Data for volute design (P=Parameter, V=Value)**

P	V	P	V	P	V
$M_i = M_1$	0.30	$R_2/b_2$	7	$\beta_2$	-38
$M_e = M_2$	0.677	$\eta_v$	0.95 & 1	$C_f$	0.0018
$\alpha_i = \alpha_1$	76	S	0.85 & 1	$m_r/m(X)$	0 & 0.05
$\alpha_e = \alpha_2$	71	$\delta$	30	$\gamma$	1.302

The magnitude of the assumed angular momentum dissipation parameter has a significant effect on the predicted radius ratio (Fig. 4) but no detectable effect on the area ratio (Fig. 5). By modifying the assumed parameter of mass flow recirculation from 0% to 5%, the predicted area ratio was modified whilst the corresponding radius ratio showed no significant change. It is clear that the assumed dissipation of angular momentum has the most significant influence on the predicted geometry, and must, therefore, be assessed accurately. The derivation of the centroid flow angle at the volute centre through the free vortex assumption is shown as a function of azimuth angle in Fig. 6. This shows an inconsistency, particularly at  $\phi = 360^\circ$  (where the radius ratio equals unity), where the calculated flow angle differs from the desired discharge flow angle of  $71^\circ$  (refer table 2). In order to modify the design so that the desired flow angle is achieved, it is necessary to modify the free vortex assumption and that through by introducing the exponent.

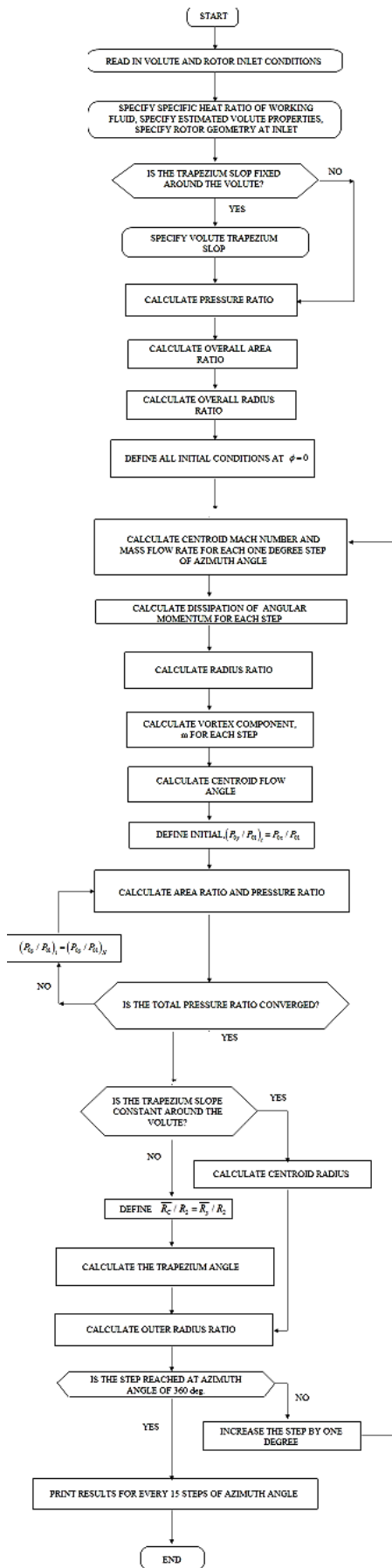


Fig. 3. Flow Diagram of Volute Design.

The vortex exponent, is introduced as a function of azimuth angle so that the free vortex flow could be modified gradually with increasing azimuth angle. The exponent is derived through the relationship [Whitfield (1991, 1994)]

$$m = m_0 - k \phi^p \quad (1)$$

where  $m_0$  is the exponent at volute inlet and  $k$  and  $p$  are constants derived from specified boundary conditions. The constant  $k$  was derived from a specified exponent,  $m_{360}$ , at  $\phi = 360^\circ$ ,

$$k = \frac{m_0 - m_{360}}{360^p} \quad (2)$$

while the constant,  $p$ , was derived from a second specified exponent,  $m_\phi$  at a specified angle, usually  $180^\circ$  or  $270^\circ$ , then

$$p = \frac{\ln \left[ \frac{m_0 - m_\phi}{k} \right]}{\ln \phi}$$

or eliminating,  $k$ , through Eqn. 2,

$$p = \frac{\ln \left( \frac{m_0 - m_\phi}{m_0 - m_{360}} \right)}{\ln \left( \frac{\phi}{360} \right)} \quad (3)$$

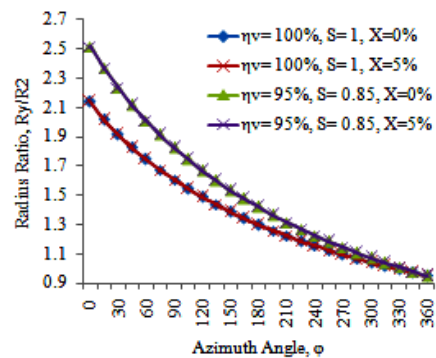


Fig. 4. Centroid radius as a function of azimuth angle with free vortex assumption.

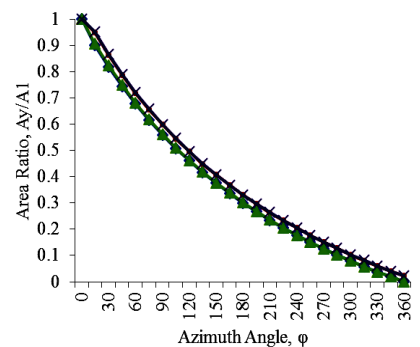
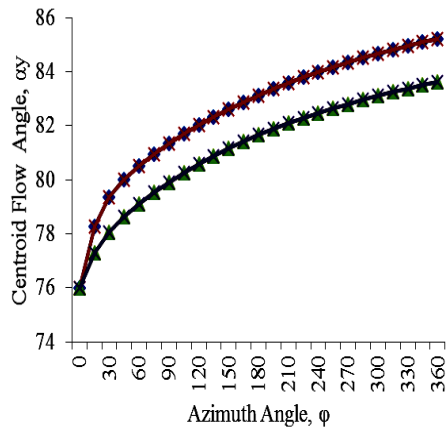
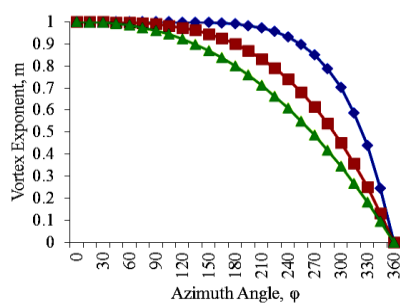


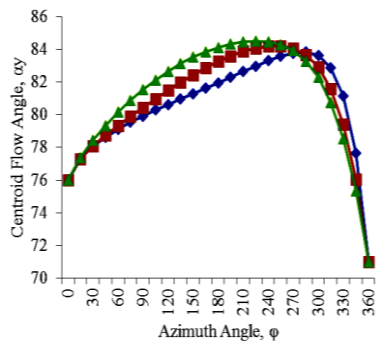
Fig. 5. Cross-Sectional area as a function of azimuth angle with free vortex assumption.



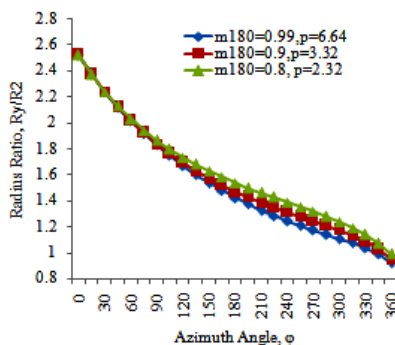
**Fig. 6. Centroid flow angle as a function of azimuth angle with free vortex assumption.**



(a)



(b)



(c)

**Fig. 7. Variation of centroid flow angle and radius ratio as a function of azimuth angle ( $m_0 = 1, m_{360} = 0$  and  $m_{180}$  as shown in legend).**

The effects of different values of exponent and different values of constant  $k$  and  $p$  on centroid flow angle and radius ratio are shown in Fig. 7. The exponent provided a flexible control on the assumed vortex flow. A near free vortex flow could be assumed over any desired azimuth angle range and then modified at a prescribed rate. Typical exponents used are shown in Figs 7(a). In all cases a free vortex is assumed initially,  $m_0 = 1$ , into Eq. 1, and the exponent then reduced in a defined manner in order to assess the effect on the volute design. At an azimuth angle of  $360^\circ$ , "m" is often assumed to be zero; this is equivalent to assuming a uniform flow through the narrow passage between the rotor periphery and the underside of the volute tongue.

The effect of three prescribed vortex exponent distributions is shown in Fig. 7(a). The effect of these distributions on the derived centroid flow angle is shown in Fig. 7(b). Each distribution has had the desired effect of reducing the flow angle over the later part of the volute, and in particular provided the correct flow angle at  $\phi = 360^\circ$  (this is due entirely to the assumption that  $m_{360} = 0$ ). The general trend of the flow angle distribution is shown in Fig. 7(b). The consequences for the predicted volute mean radius ratio is shown in Fig. 7(c), whilst the effect on the area ratio is not significant, hence not shown. Of the three distributions shown the one given by  $p=6.64$ , is probably more realistic than the other two as it maintains a free vortex distribution over the first 180 degrees of azimuth angle and hence it is selected to design the volute. The non-dimensional area ratio is then converted in dimensional form for 25kW capacity gas turbine. Fig. 8 shows the 3-D actual volute and cross section area of designed volute.

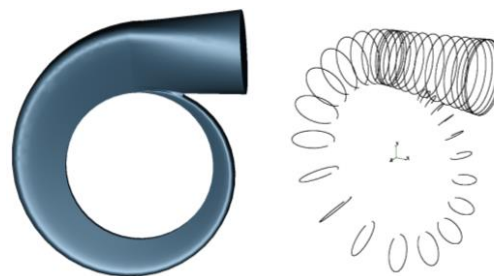


**Fig. 8. 3-D model and cross section of volute at different azimuth angle.**

Prior to experimentation, it is required to evaluate a performance of designed turbine in detail. Accordingly, the simulation of designed turbine is carried out using commercially available CFD code for computational validation of alternate design philosophy.

### 3. NUMERICAL SIMULATION

#### 3.1 Computational Domain

The commercially available finite volume Navier-Stokes solver (ANSYS-CFX) is used to obtain the

computational results. As the stage performance can be heavily influenced by the turbine inlet conditions, it is decided to develop full numerical model including rotor to obtain a detailed description of the rotor inlet flows. To resolve time dependent features within rotor full 3D transient simulation is performed. Care has been taken for  $Y^+$  values during meshing, which lies in the range of 20-100. Mesh statistics, after grid independence, of each subdomain and generated structural mesh are presented in Fig. 9. Wall function approximation of boundary layer flow is done by applying SST turbulence model. The combination of mass flow rate at the inlet and static pressure at the outlet has been found to provide good numerical stability and convergence rates in radial turbine simulations. The detailed summary of boundary condition used is shown in Table 5. The rotating frame of reference requires performing the simulation in transient conditions accordingly, in current simulations, a time step size of 120 time steps per rotor revolution was considered. Therefore, for the given rotational speed of the impeller, the time step size is  $3.33e-05$  seconds.

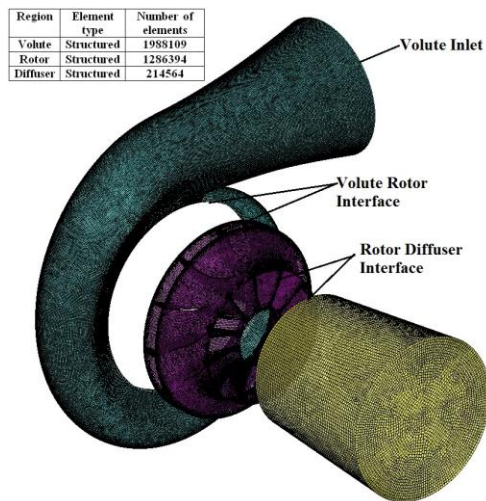


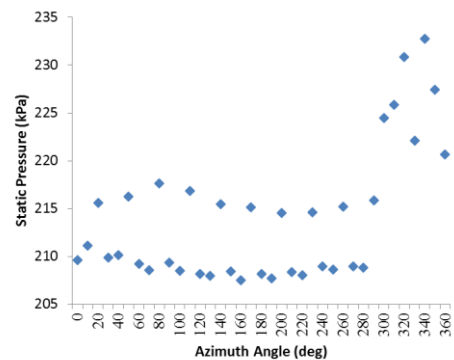
Fig. 9. Exploded view of computational domain.

Table 5 Summary of boundary conditions

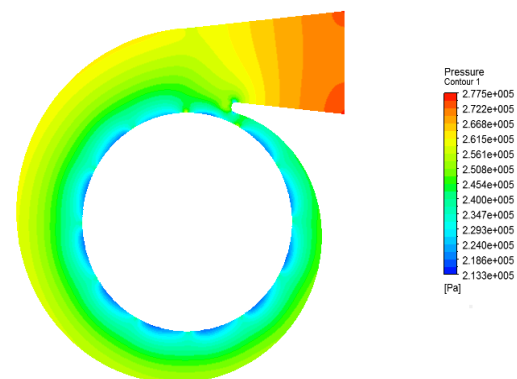
Boundary type	Location	Specified condition
Inlet	Volute Entry (upper-lower)	Mass flow rate Total Temperature
Outlet	Diffuser exit	Averaged static pressure
Wall	Rotor hub, shroud, blades Volute and diffuser duct	Smooth, no slip
Grid interface	Volute exit-rotor inlet Rotor exit-Diffuser inlet	Conservation flux Transient rotor - stator

### 3.2 Pressure Variation

As mentioned previously, to get the actual value of static pressure, the turbine blades are modeled using a transient rotor-stator interface. In this way a time averaged prediction of the rotor inlet flow field could be obtained. The predicted static pressure variation resulting from a transient rotor simulation is shown in Fig. 10. The non uniformity is most prominent just downstream of the tongue region, where boundary layers build up on either side of the tongue producing a distinct wake due to which spike in static pressure is around 25000 Pa at an azimuth angle of  $330^\circ$ . At rotor inlet these flow fields will only be partially mixed, non uniform and inherently unsteady.



(a)



(b)

Fig. 10. Predicted time averaged static pressure contours (center plane) in volute using a transient rotor – stator interface.

### 3.3 Comparison of CFD with Modified Free Vortex Design

In the modified free vortex design the total losses are incorporated. It should be noted that the flow is no longer free vortex after the losses are taken into account. The results presented in Figs 11-13 are only for design mass flow rate. Figure 11 compares the Mach number and flow angle variations at the geometrical centre of sectional surfaces between CFD and the modified free vortex approach. A good agreement of the Mach number variation is observed. The higher Mach numbers from CFD indicate that the centroid flow has accelerated more owing to the smaller area to radius ratio.

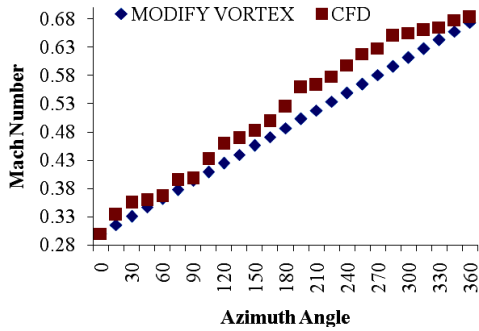


Fig. 11. Mach number variation.

Figure 12 depicts the Mach number distribution in a mid span plane through the vaneless volute of radial inflow turbine. From figure, it can be seen that the flow accelerates uniformly from the inlet duct to the exit region; however, once the passage begins to curve, higher velocities develop on the inside of the bend as the trailing edge of the tongue is approached. The influence of the tongue region is clearly depicted, showing lower momentum flow entering the rotor in this region as a consequence of the wake from the tongue and the mixing of the inlet flow with the flow emerging from under the tongue that has circled the entire rotor. The impact of the wake and mixing from the tongue does not extend any further than an azimuth angle of around 330 deg; beyond this, the volute is seen to deliver excellent uniformity over the remainder of the rotor circumference, delivering flow to rotor inlet at a Mach number of around 0.683 whereas calculated Mach number by alternate methodology is 0.677.

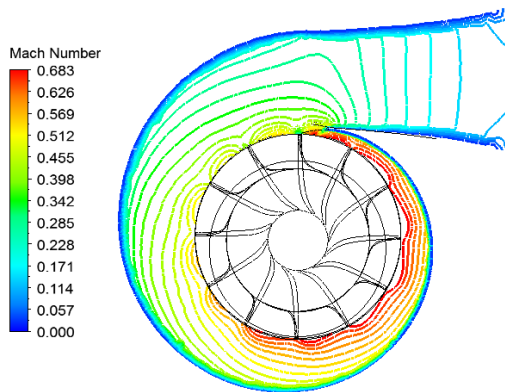


Fig. 12. Mach number distribution in the mid span plane of the vaneless volute.

The centroid flow angle predicted by CFD follows tendency of modified free vortex design as shown in Fig. 13. Of particular interest are, the radical changes in the Mach numbers upstream of the tongue ( $\phi = 330^\circ$  to  $360^\circ$ ) and the significant deviation of the centroid flow angle upstream and downstream of the tongue. These phenomena are caused by the strong acceleration around the tongue, by the wake flow from the tongue and probably by the interaction of the recirculating flow under the tongue with the main flow as explained earlier.

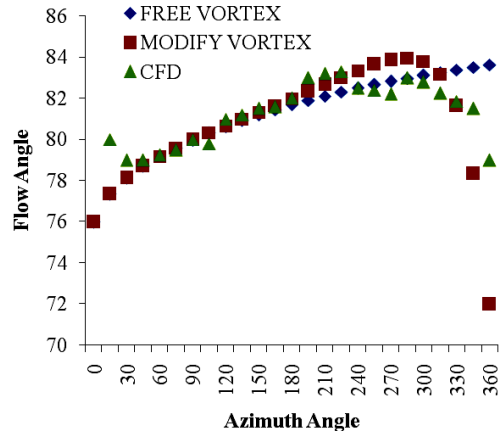


Fig. 13. Centroid flow angle variation.

Table 6 shows the comparison between results of alternate approach and CFD. It is observed that parameters like pressures, temperatures, power, mass flow rate etc. from alternative approach are in good agreement with CFD analysis. Deviations between the results are nearer or below  $\pm 5\%$ , suggest that the alternate methodology of radial turbine design gives good aerodynamic solution. The total to static efficiency of turbine by alternate approach is 84.91%, and by CFD analysis is 85.77%, which suggests that developed one dimensional alternate design methodology predict turbine efficiency very accurately at early stage of design.

Table 6 Comparison of different CFD variables with alternate approach (V=Variable, AA=Alternative Approach, %D =Deviation)

V	AA	CFD	% D
$P_2$	2.11	2.13	0.94
$P_3$	1.1	1.07	-2.80
$P_{02}$	2.82	2.82	0.00
$P_{03}$	1.15	1.12	-2.59
$T_2$	1122	1122	-0.03
$T_3$	1006	960	-4.79
$T_{02}$	1200	1200	0.00
$T_{03}$	1023	1003	-2.06
$\Delta h_0$	302.43	298.6	-1.28
$\rho_2$	0.611	0.638	4.23
$\beta_2$	-38	-37	-2.70
$M_2$	0.677	0.683	0.88
$M_3$	0.33	0.318	-3.77
$P$	25	26.23	4.69
$\eta_{ts}$	84.91	85.77	1.00
$\dot{m}$	0.1028	0.103	0.19

#### 4. EXPERIMENTAL INVESTIGATIONS

##### 4.1 Introduction

To rate the performance by giving load on the high speed turbine using the methodology suggested in literature (Whitfield (1994), MacGregor (1994), Kofskey (1966, 1969, 1972), Futral (1970 a,b), Choo (1985), Mclallin (1980), Barr (2009)) requires high speed dynamometer and other accessories. The rotational speed of 150000 rpm is very large to be handled directly by the equipment. To overcome this, many researchers (Futral (1965), Ghassemi (2005), Spence (1997, 2007), Artt (1998), Payri (2012), Deng (2007), Gallus (1992), Simpson (2009), Aghaali (2008), Hajilouy (2009)) have given the loading using air brake. The air brake is indirectly but compressor load, for which the initial and final state points of pressure and temperature are measured across the turbine and the load is calculated mathematically. Employing a concept similar to above, the designed turbine is manufactured on 5 axis milling machine and employed in similar turbocharger available in the market so that the adequate performance can be predicted. The limitations of surging and choking in compressor as well as in the bearings to take up load at such high speeds, allowed the tests to be conducted up to 70000 rpm only. Accordingly, a turbine test rig was constructed to facilitate the accurate measurement of the gas temperature and pressure entering and leaving the turbine stage. The turbine work was determined from the turbine temperature drop rather than compressor work or dynamometer torque.

##### 4.2 Experimental Setup

Fig. 14 and 15 shows the layout of the turbine stage. The static pressure at rotor inlet was measured using static pressure tapings just before to the turbine volute. The temperatures were measured using K type thermocouple procured from United Sensor. A computerized data-acquisition system was used to record temperature data. A simple analysis showed that the maximum gas velocity at location of thermocouple during the test program was 46.65 m/s. These velocities corresponded to a dynamic temperature head of 0.805 K and a pressure head of 689 Pa (0.0689 bar). Therefore any errors arising from the dynamic head were negligible. Air delivery to the combustion chamber was provided by adjustment of the pressure regulating valve. An orifice plate was installed and used in accordance with IS 14615-1 to measure the mass flow rate through the turbine. A kerosene fuelled combustion chamber heated the air entering the turbine. All tests were conducted with a turbine inlet temperature in order of 750K to 1000K and an atmospheric exit pressure. The turbine load was mainly controlled by adjustment of the load by compressor delivery valve. Uncertainties were estimated as the sum of observation errors and instrument errors. In the case of observation errors, the recommendations given by Topping (2012) were adopted. The total estimated uncertainty in total to static efficiency is

$\pm 1.734\%$  at design point and it increases as turbine runs at off-design.

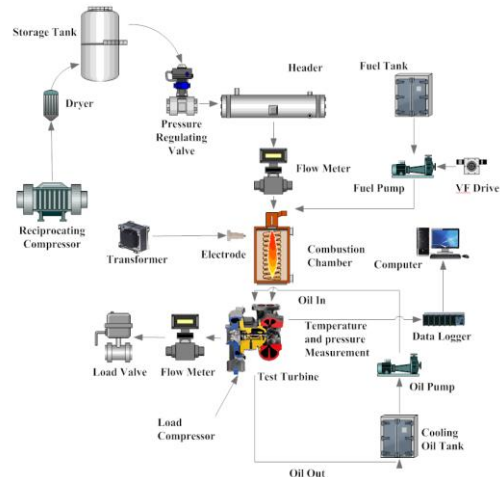


Fig. 14. Schematic layout of radial turbine test rig.

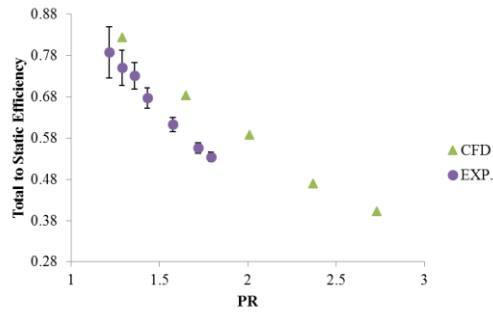


(1- compressor, 2- air receiving tank, 3- PRV, 4, 5- flow meters, 6- pressure tapping, 7- pressure gauge, 8- test turbine, 9- load compressor, 10- cooling oil in, 11- cooling oil out, 12- spark electrode, 13- fuel supply, 14- thermocouples, 15- data logger, 16- load valve, 17- cooling oil pump, 18- cooling oil tank, 19- flow totalizer, fuel supply tank, 21- fuel pump assembly)

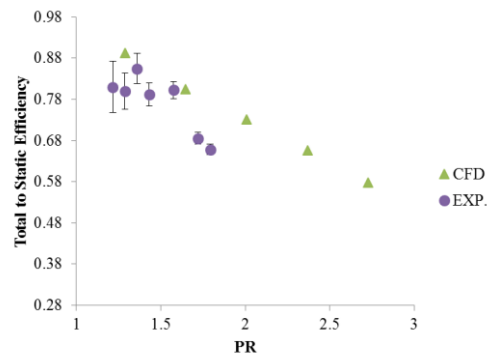
Fig. 15 Layout of radial turbine test rig.

##### 4.3 Results and Discussions

The range of turbine operation is narrow if compared with the results of CFD due to limitation on compressor side. The turbine operating range covered during the tests is up to 70000 rpm only. The turbine inlet temperature, was not directly controlled and therefore varied according to the flow rate in combustion chamber, from an average of about 700K to 1000K at turbine speed of 50000 rpm to about 70000 rpm. It can be seen that the results were obtained in the ranges  $0.0431 < \dot{m} < 0.0915$  kg/s and  $1.19 < PR < 1.79$ , which corresponded to a turbine output between 1.69 kW to 10.22kW. The results illustrated in Figs 16 to 21 are at 900K – 50480 rpm and at 1000K – 69860rpm.



**Fig. 16. Total to static efficiency versus pressure ratio at 50480 rpm (Tin=900K).**



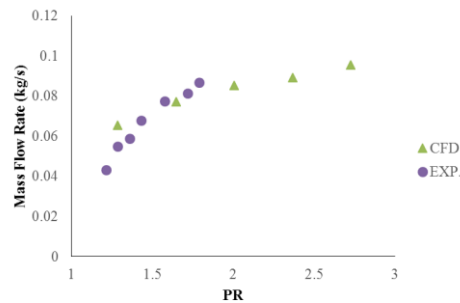
**Fig. 17. Total to static efficiency versus pressure ratio at 69860 rpm (Tin=1000K).**

Figure 16 and 17 shows the total to static efficiency versus pressure ratio at 50480 rpm and 69860 rpm, respectively. The uncertainty band is in the range of  $\pm 13.76\%$  to  $\pm 3.12\%$  for pressure ratio ranging from 1.19 to 1.79. It is worth to observe that the predicted CFD results are in good agreement with test results.

The Fig. 16 suggests that CFD models over predicted total to static efficiency by order of 7-8%. These deviations are reduced as turbine runs close to design point as reflected in Fig. 17. The performance predicted by CFD is close to experimental prediction up to pressure ratio of 1.79. Beyond this pressure ratio no experimental data is available for validation. The extrapolation of these curves may construct the performance map beyond pressure ratio of 1.79 but it introduces uncertainty in to the prediction and hence, not introduced. As will be seen, the values of total-to-static efficiency predicted by CFD analysis are always higher than the test results. Some possible reasons are proposed hereafter. Firstly, in view of the fact that the Reynolds number would not be larger than the order of  $10^5$  for the general working fluid. Most of the loss correlations in CFD analysis are developed from the experimental results and experience for which the corresponding Reynolds number lies within the order of  $10^4$ - $10^5$ . However, with regard to the fluid properties of gas turbine, the 25 kW radial inflow turbine characteristics over the full operating range are based on the Reynolds number which lies within the order of  $10^6$ - $10^7$ . Due to the lack of corrected parameter for Reynolds number in

the loss correlation system, it will cause errors in the efficiency predictions by CFD analysis. Thus, if the loss correlation system is based on the eligible order of Reynolds number for the real working fluid, the results will become closer to the real situation.

As seen from Figs. 18 and 19, the trend in stage mass flow rate is very similar for the CFD curves and test results. However, as seen from the CFD prediction, many kinks exist in these curves at low pressure ratio. The reason for these kinks is that the poor convergence in the CFD analysis at low pressure ratio and therefore the result accuracy at this point is reduced. The difference between the results of mass flow rates of CFD and the experiments is quite small at lower stage expansion ratio and it increases at higher stage expansion ratio.



**Fig. 18. Mass flow rate versus pressure ratio at 50480 rpm (Tin=900K).**

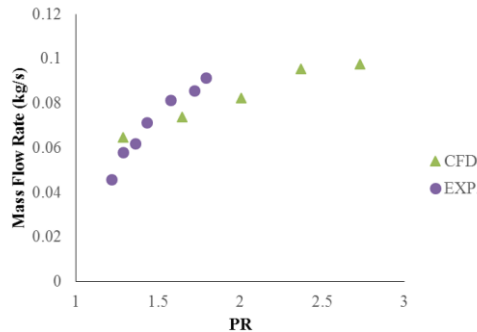


**Fig. 19. Mass flow rate versus pressure ratio at 69860 rpm (Tin=1000K).**

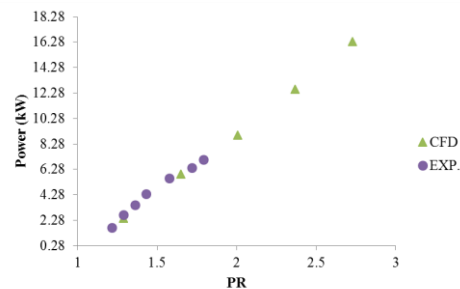


**Fig. 20. Power versus pressure ratio at 50480 rpm (Tin=900K).**

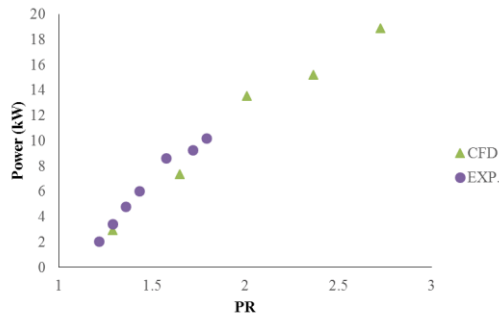


**Fig. 21. Power versus pressure ratio at 69860 rpm ( $T_{in}=1000K$ ).**

At pressure ratio higher than 1.79, the stage mass flow rate increases gradually with the increase in pressure ratio. The power predicted by CFD is closely matched with experimental results as shown in Figs. 20 and 21. The uncertainty in power measurement is ranging from 0.873% to 2.49%, which corresponded to a turbine output between 1.69 kW to 10.22 kW. As the pressure ratio increases the power developed by turbine also increases. However in present study for pressure ratio higher than 1.79, no experimental data is available for validation.

## 5. CONCLUSIONS

The work reported arose from an interest in developing high efficiency turbines for small gas turbine applications. The objective is to develop a unified methodology to design a radial turbine. The main part of design combines one dimensional calculation by applying thermodynamic and gas dynamics fundamentals. The developed procedure is intended as a simple and robust integrated process. The salient features of the work are summarized as below:

1. The alternate turbine design procedure gives a good aerodynamic solution and does not rely on specific assumptions and does not suffer from limitations of existing literature. From the alternate design approach turbine total to static efficiency is 84.91% and 85.77% by CFD simulation.
2. The design method is extended to include vaneless volute housing. It has been shown that free vortex pattern is a fair approximation over the first 180 degrees of azimuth angle only. The free vortex assumptions are inapplicable, particularly at tongue region, where calculated centroid flow angle differs from the desired flow angle of  $71^\circ$ . Over the later part of the volute (i.e. after  $180^\circ$ ), the free vortex assumption is, therefore, replaced by vortex exponent as a function of azimuth angle and it approaches to zero at 360 degrees azimuth angle, which finally confirm flow angle of  $71^\circ$  at tongue.
3. A designed turbine is validated by CFD investigation and thermodynamic parameters are found to be in good agreement with  $\pm 5\%$

deviation.

4. A developed turbine is tested to validate alternate design approach. The developed test facility was able to test turbine upto a speed of 70000 rpm, at turbine inlet temperatures ranging from 700 K to 1000 K and upto a pressure ratio of 1.79, which developed power in the range of 1.69 kW to 10.22 kW. The uncertainty band is in order of  $\pm 13.76\%$  to  $\pm 3.12\%$ . It is observed that the CFD results are in good agreement with test results at off design condition.

Finally, it may be stated that the present work provides a unique design method for radial inflow gas turbines. The alternate philosophy is applied and validated by 3D CFD simulation and experimentations at part load conditions. Thus, alternate design philosophies can be used to design radial turbines with confidence.

## ACKNOWLEDGEMENTS

I would like to thank GUJCOST for financial support.

## REFERENCES

- Aghaali, H. and A. Hajilouy-Benisi (2008). Experimental Modeling of Twin-Entry Radial Turbine. *Iranian Journal of Science and Technology* 32, 571.
- Artt, D. W. and S. W. T Spence (1998). A Loss Analysis Based on Experimental Data for a 99.0mm Radial Inflow Nozzled Turbine with Different Stator Throat Areas. *Proceedings of the Institution of Mechanical Engineers* 212.
- Atkinson, M. J. (1998). *The design of efficient radial turbines for low power applications*. Ph.D. Report, University of Sussex.
- Baines, C (1996). Flow development in radial turbine rotors. In *International Gas Turbine and Aeroengine Congress and Exhibition*, ASME.
- Balje, O. E. (1962). A study on design criteria and matching of turbomachines: Part A—Similarity relations and design criteria of turbines." *Journal of Engineering for Power* 84 (1), 83-102.
- Barr, L., S. Spence and D. Thornhill (2009 June). A Numerical and Experimental Performance Comparison of an 86 mm Radial and Back Swept Turbine. *Proceedings of ASME Turbo Expo 2009: Power for Land, Sea and Air, GT2009*, Orlando, Florida, USA.
- Chen, H. and N. C. Baines (1994). The aerodynamic loading of radial and mixed-flow turbines." *International Journal of Mechanical Sciences* 36 (1), 63-79.
- Choo, Y. K. and K. C. Civinskas (1985). Three-Dimensional Inviscid Analysis of Radial

- Turbine Flow and a Limited Comparison with Experimental Data. *NASA TM-87091*.
- Deng, Q. J. N., J. Mao and Z. Feng. (2007). Experimental and Numerical Investigation on Overall Performance of a Radial Inflow Turbine for 100kW Microturbine. *ASME Turbo Expo 2007: Power for Land, Sea, and Air* 919-926.
- Futral, S. M. and C. A. Wasserbauer (1965). Off-design Performance Prediction with Experimental Verification for a Radial-Inflow Turbine. *NASA TN D-2621*.
- Futral, S. M. and C. A. Wasserbauer (1970a). Experimental Performance Evaluation of a 4.59-Inch Radial-Inflow Turbine with and without Splitter Blades. *NASA TN D-7015*.
- Futral, S. M. and D. E. Holeski (1970b). Experimental Results of varying the Blade-Shroud Clearance in a 6.02-inch Radial Inflow Turbine. *NASA Technical Note D-5513*.
- Gallus, H. E., U. Lingner and I. Ispas (1992). Experimental Analysis of Transonic Flow through the Variable Nozzle of a Radial Inflow Turbine. *ASME Paper*, 92- GT -90.
- Ghassemi, S., E. Shirani and A. Hajilouy-Benisi (2005). Performance Prediction of Twin-Entry Turbocharger Turbines. *Iranian Journal of Science & Technology, Transaction B, Engineering* 29.
- Glassman, A. J. (1976). Computer program for design analysis of radial-inflow turbines. *NASA TN D-8164*.
- Gu, F., A. Engeda, and E. Benisek (2001). A comparative study of incompressible and compressible design approaches of radial inflow turbine volutes. *Proceedings of the Institution of Mechanical Engineers, Part A: Journal of Power and Energy* 215(4), 475-486.
- Hajilouy-Benisi, A., M. Rad, M. R. Shahhosseini (2009). Flow and Performance Characteristics of Twin-Entry Radial Turbine under full and Extreme Partial Admission Conditions. *Archive of Applied Mechanics* 79, 1127-1143.
- Hiatt, G. F. and Johnston I. H. (1963). Experiments concerning the aerodynamic performance of inward flow radial turbines. *In Proceedings of the Institution of Mechanical Engineers* 178 (9), 28-42.
- Kofsky, M. G. and C. A. Wasserbauer (1966). Experimental Performance Evaluation of a Radial-Inflow Turbine Over a Range of Specific Speeds. *NASA TN D-3742*.
- Kofsky, M. G. and C. A. Wasserbauer (1969). Experimental Evaluation of a 3.50-Inch Radial Turbine Designed for a 10-Kilowatt Space Power System. *NASA TN D-5550*.
- Kofsky, M. G. and W. J. Nusbaum (1972). Effects of Specific Speed on Experimental Performance of a Radial-Inflow Turbine. *NASA TN D-6605*.
- MacGregor, S. A., A. Whitfield, and A. B. Mohd Noor (1994). Design and performance of vaneless volutes for radial inflow turbines: part 3: experimental investigation of the internal flow structure. *Proceedings of the Institution of Mechanical Engineers, Part A: Journal of Power and Energy* 208(4), 295-302.
- McLallin, K. L. and J. E. Haas (1980). Experimental Performance and Analysis of 15.04-CM-Tip-Diameter, Radial Inflow Turbine with Work Factor of 1.126 and Thick Blading. *NASA TP-1730*.
- Payri, F., J. R. Serrano, P. Fajardo, M. A. Reyes-Belmonte and R. Gozalbo-Belles (2012). A Physically Based Methodology to Extrapolate Performance Maps of Radial Turbines. *Energy Conversion and Management* 55, 149-163.
- Rodgers, C. (1987a). High pressure ratio turbine design constraints. *Von Karman Inst. for Fluid Dynamics, Small High Pressure Ratio Turbines*, 1987.
- Rodgers, C. and R. Geiser (1987b). Performance of a high-efficiency radial/axial turbine. *Journal of turbomachinery* 109 (2), 151-154.
- Rohlik, H. E. (1975). Radial-inflow turbines, Turbine design and application. *NASA SP-290, Vol. 3, Chapter 10*.
- Simpson, T. S., W. T. Spence and J. Early (2009 June). A Numerical and Experimental Study of the Rotor Inlet Flow Fields of Radial Turbines using Vaned and Vaneless stators. *Proceedings of ASME Turbo Expo 2009: Power for Land, Sea and Air* Orlando, Florida, USA.
- Spence, S. W. T. and D. W. Artt (1997). Experimental Performance Evaluation of a 99.0 mm Radial Inflow Nozzled Turbine with Different Stator Throat Areas. *Proceedings of the Institution of Mechanical Engineers* 211.
- Spence, S. W., R. S. Rosborough, D. Artt, and G. McCullough (2007). A direct performance comparison of vaned and vaneless stators for radial turbines. *Journal of turbomachinery* 129 (1), 53-61.
- Topping, J. (2012). Errors of Observation and their Treatment. *Springer Science & Business Media* 62.
- Watanabe, I., I. Ariga, and T. Mashimo (1971). Effect of dimensional parameters of impellers on performance characteristics of a radial-inflow turbine. *Journal of Engineering for Power* 93(1), 81-102.
- Wei, Z. (2014). *Meanline analysis of radial inflow turbines at design and off-design conditions*. Ph.D. Report, Carleton University Ottawa.
- Whitfield, A (1989). The preliminary design of radial inflow turbines. *International Gas Turbine and Aeroengine Congress and*

- Exposition*, American Society of Mechanical Engineers.
- Whitfield, A. and A.B. Mohd Noor (1991). A non-dimensional conceptual design procedure for the vaneless volutes of radial inflow turbines. *International Gas Turbine and Aeroengine Congress and Exposition*, American Society of Mechanical Engineers, 1991.
- Whitfield, A., S. A. MacGregor and A.B. Mohd Noor (1994). Design and performance of vaneless volutes for radial inflow turbines: part 2: experimental investigation of the mean line performance assessment of empirical design parameters. *Proceedings of the Institution of Mechanical Engineers, Part A: Journal of Power and Energy* 208(3), 213-224.